Open-Loop Impedance Control for the Open-Source Prosthetic Leg: Characterization, Compensation, and Validation

T. Kevin Best, Gray C. Thomas, Senthur Raj Ayyappan, Robert D. Gregg, and Elliott J. Rouse

***Abstract*— Abstract TODO, it'll be awesome**

I. Introduction

Although powered prostheses may help alleviate some of the problems with conventional microprocessor prosthetic legs, control of these devices remains a challenge.

The open source leg (OSL) project aims to address this challenge by lowering the barrier to entry for prosthetic leg controls research [1].

Open-loop impedance control is commonly used for robotic prostheses [2]–[4]. However, unmodeled drivetrain dynamics can affect the output impedance at the joint, causing incorrect joint torques. Closed-loop impedance control (*i.e.* adding a sensor to directly measure output torque) can solve this problem, but cost and weight concerns usually make this approach infeasible. Alternatively, model-based compensation can be used to account for drivetrain dynamics and improve output torque accuracy.

The goal of this work is to model and compensate for the drivetrain dynamics of the OSL.

This paragraph will overview the planned organization of the paper, which I will probably remove. Section II details the drivetrain components and their mathematical models. In Section III, we develop an impedance compensator and experimentally validate it on a mechanical dynomometer. Finally, Section IV details a walking experiment in which we again experimentally determine the joint impedance while the OSL was walked on by an amputee participant.

II. Model of Drivetrain Dynamics

A. Hardware Overview

The OSL drivetrain (Fig. 1) consists of an off-the-shelf exterior rotor actuator (Dephy Actpack 4.1, Maynard, MA) coupled with a single stage belt transmission (Gates TODO).

B. Actuator and Transmission Models

1) Actuator Model: This actuator has been extensively characterized in previous work [5], [6]. In [6], the authors regressed a model to the actuator's output torque τ_m and found that the behavior is well described by

$$\tau_\mathrm{m} = I_q k_\tau n_\mathrm{m} - f(\dot{\theta}_\mathrm{m}, I_q) - B_\mathrm{m}\dot{\theta}_\mathrm{m} - J_\mathrm{m}\ddot{\theta}_\mathrm{m}, \qquad (1)$$

where I_q is the q-axis motor current, k_τ is the corresponding torque constant, n_m is the gear ratio of the actuator, $\dot{\theta}_\mathrm{m}$ and $\ddot{\theta}_\mathrm{m}$ are the actuator's output velocity and acceleration, respectively, and B_m and J_m represent output viscous damping and inertial constants, respectively. Motor friction $f(\dot{\theta}_\mathrm{m}, I_q)$ is modeled as

$$f(\dot{\theta}_\mathrm{m}, I_q) = \mathrm{sign}(\dot{\theta}_\mathrm{m})\left(f_C + f_G|I_q|\right), \qquad (2)$$

where f_C and f_G parameterize coulomb and gear friction behaviors, respectively. In short, the motor torque is dictated primarily through motor current, friction, and inertia. The parameters of the actuator model are listed in Table I.

2) Transmission Model: Using the framework presented in [7] for a series-elastic actuator, the actuator output angle θ_m is related to the joint angle θ_j as

$$\theta_\mathrm{j} = \theta_\mathrm{m}/n_\mathrm{T} + \theta_\mathrm{s}, \qquad (3)$$

where θ_s is the effective angular deflection of the transmission with gear ratio n_T.

The transmission was modeled as an inertia with viscous damping connected in parallel to an elastic element with stiffness K_s connected to the input. The output torque at the joint τ_j is therefore

$$\tau_\mathrm{j} = -K_\mathrm{s}\theta_\mathrm{s} - B_\mathrm{j}\dot{\theta}_\mathrm{j} - J_\mathrm{j}\ddot{\theta}_\mathrm{j}. \qquad (4)$$

The physical parameters of the model $(K_\mathrm{s}, B_\mathrm{j}, J_\mathrm{j})$ were identified using a custom rotary dynamometer (motor: Baldor

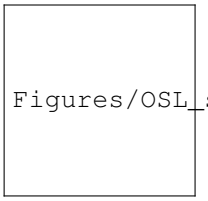

Fig. 1. Schematic, cutaway, or something similar showing the OSL drivetrain architecture.

TABLE I
Actuator and Transmission Model Parameters

n_m	9.0		n_T	83/11
k_τ	113.3 $\times 10^{-3}$ Nm/A		K_s	685.9 Nm/rad
B_m	5.6 $\times 10^{-3}$ Nms/rad		B_j	45.2 $\times 10^{-2}$ Nms/rad
J_m	9.211 $\times 10^{-3}$ Kg m^2		J_j	5.0 $\times 10^{-3}$ Kg m^2
f_C	37.7 $\times 10^{-2}$ Nm		f_G	89.6 $\times 10^{-3}$ Nm/A

This work was supported by TODO. The content is solely the responsibility of the authors and does not necessarily represent the official views of the NIH or NSF.

TODO

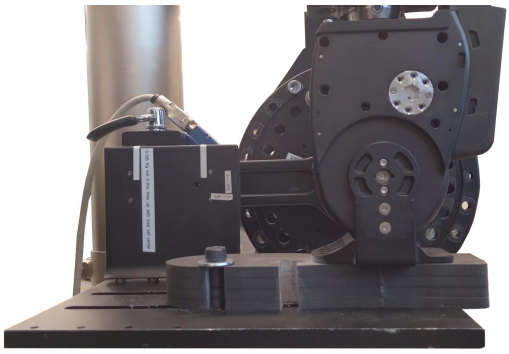

Fig. 2. Photo of the OSL ankle mounted in the dynamometer. The OSL shank and foot are both rigidly attached to the dynamometer, allowing purely rotational motion. A thick footplate was constructed in order to align the rotation axes of the dynamometer and the ankle.

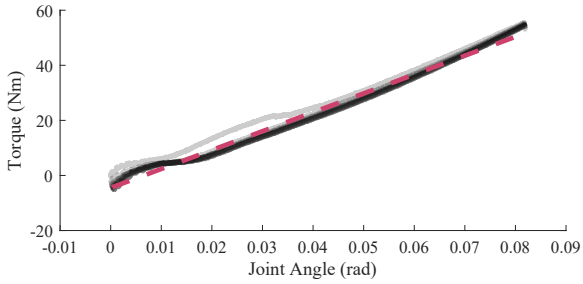

Fig. 3. Torque-deflection plot of the OSL transmission over ten individual trials (transparent gray). The average belt stiffness was identified using least squares to be 685.6 Nm/rad (magenta dashed).

BSM90N-3150AF; load cell: JR3 45E15A4). The OSL ankle rigidly attaches to the dynamometer at the shank and the foot, allowing a single rotational degree of freedom about the ankle axis (Fig. 2).

First, the transmission belt stiffness, defined as the slope of the torque-deflection curve during loading, was characterized by locking the input shaft and moving the joint output 5 deg. The experiment was repeated ten times and the slope of the torque-deflection curve was calculated using least squares. Averaged over ten trials (Fig. 3), $K_\mathrm{s} = 685.6$ Nm/rad.

Next, B_j and J_j were identified in dynamic trials. With the motor detached ($\theta_\mathrm{s} = 0$), the dynamometer drove the joint angle with a stepped sinusoidal signal ($f \in \{1, 2, 3, 4, 5\}$ Hz, 20 cycles per frequency) at amplitudes of 2, 4, and 6 deg, repeated 5 times. Using least squares regression, the torque response was fit to the transmission model (4) with an average variance accounted for (VAF) of 99.1%. The torque response was dominated by viscous damping effects, with $B_\mathrm{j} = 45.2 \times 10^{-2}$ Nms/rad and J_j negligible (Table I).

III. Output Impedance Compensation

A. Controller Design

1) Feedback Linearization: The high quality motor model allows us to use feedback of the motor's state to linearize the motor dynamics. To replace the motor's natural dynamics with simpler second order dynamics with a new control input u, let

$$I_q = \frac{u + f(\dot{\theta}_\mathrm{m}, I_q)}{k_\tau n_\mathrm{m}}. \tag{5}$$

Substituting into (1), the torque at the output of the actuator becomes linear with the new control input u:

$$\tau_\mathrm{m} = u - B_\mathrm{m}\dot{\theta}_\mathrm{m} - J_\mathrm{m}\ddot{\theta}_\mathrm{m}. \tag{6}$$

Finally, if we implement a standard impedance feedback controller on the motor angle with stiffness K_1, damping B_1 and equilibrium angle θ_eq, the motor dynamics become

$$\tau_\mathrm{m} = K_1\left(\theta_\mathrm{eq} - \theta_\mathrm{m}\right) - B_1\dot{\theta}_\mathrm{m} - B_\mathrm{m}\dot{\theta}_\mathrm{m} - J_\mathrm{m}\ddot{\theta}_\mathrm{m}. \tag{7}$$

Note that through a change of variables, θ_eq can be eliminated, so it will be neglected going forward without loss of generality. The tunable gains K_1 and B_1 remain as design choices.

2) Gain Selection: The system dynamics of the full drivetrain can be described in the frequency domain as

$$\begin{aligned} &\theta_\mathrm{j} = \theta_\mathrm{m}/n_\mathrm{T} + \theta_\mathrm{s}, \quad \tau_\mathrm{j} = -K_\mathrm{s}\theta_\mathrm{s} - B_\mathrm{j}\dot{\theta}_\mathrm{j} - J_\mathrm{j}\ddot{\theta}_\mathrm{j}, \\ &\tau_\mathrm{s} = K_\mathrm{s}\theta_\mathrm{s}, \quad \tau_\mathrm{m} = -\tau_\mathrm{s}/n_\mathrm{T}. \end{aligned} \tag{8}$$

Algebraic manipulation of the system dynamics (8) with the feedback-linearized motor dynamics (7) yields the closed loop joint integral admittance $Y(s) = -\theta_\mathrm{j}/\tau_\mathrm{j}$, given by

$$Y(s) = \frac{J_\mathrm{m}s^2 + (B_\mathrm{m} + B_1)s + K_1 + K_s/n_\mathrm{T}^2}{d_3 s^3 + d_2 s^2 + d_1 s + d_0}, \tag{9}$$

where

$$\begin{aligned} d_3 &= J_\mathrm{m}B_\mathrm{j}, \\ d_2 &= (B_\mathrm{m} + B_1)B_\mathrm{j} + K_\mathrm{s}J_\mathrm{m}, \\ d_1 &= K_\mathrm{s}(B_\mathrm{m} + B_1) + (K_1 + K_\mathrm{s}/n_\mathrm{T}^2)B_\mathrm{j}, \\ d_0 &= K_1 K_\mathrm{s}. \end{aligned} \tag{10}$$

Given a desired joint stiffness K_d and damping B_d, a desired integral admittance $Y_d(s)$ can be defined as

$$Y_d(s) = \frac{1}{B_d s + K_d}. \tag{11}$$

We desire to select the control gains K_1 and B_1 such that $Y(s)$ behaves as similarly as possible to $Y_d(s)$. First, we can select K_1 so that the system has the correct DC gain, *i.e.* $Y_d(0) = Y(0)$:

$$\frac{1}{K_d} = \frac{K_1 + K_\mathrm{s}/n_\mathrm{T}^2}{K_1 K_\mathrm{s}}, \tag{12}$$

$$K_1 = \frac{K_d K_\mathrm{s}}{n_\mathrm{T}^2(K_\mathrm{s} - K_d)}. \tag{13}$$

We select the remaining gain B_1 to give the best possible approximation of the desired admittance. Let the difference between the desired and actual admittance be $\tilde{Y}(s) = Y(s) - Y_d(s)$. Let $W(s)$ be a lowpass filter (3rd order butterworth, $\omega_c = 1$ Hz) used to discount high frequency errors. In order for the system to produce an admittance as closed to the desired as possible, we select B_1 as

$$\min_{B_1} \quad ||W(s)\tilde{Y}(s)||_2 \tag{14}$$

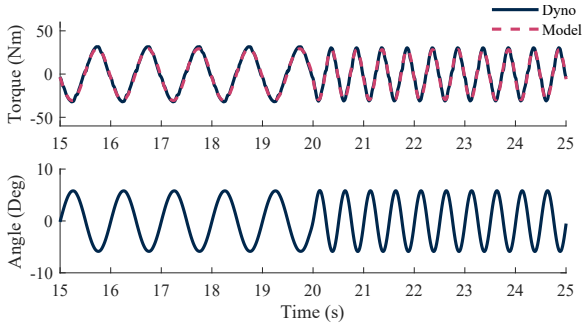

Fig. 4. Example timeseries data for a 10 s subsection of a dynomometer validation trial. In this trial, $K_d = 300$ Nm/rad and $B_d = 5$ Nms/rad. The blue dashed line shows the best fit second-order system.

A gradient descent optimization routine was constructed to solve (14), though it may have an analytical solution. Not sure if it's convex but I don't think so.

B. Dynamometer Validation

A dynamometer experiment was conducted to validate the controller's ability to render a desired joint impedance and to demonstrate the controller's benefit over a non-compensated system. The experiment was repeated twice, once using the impedance compensation methods discussed above and once neglecting all drivetrain dynamics (*i.e.* $\tau_\text{m} = -K_d\theta_\text{m} - B_d\dot{\theta}_\text{m}$).

In each trial, the dynamometer drove the joint angle with a stepped sinusoidal signal ($f \in \{1, 2, 3, 4, 5\}$ Hz, 20 cycles per frequency) at amplitudes of 2, 4, and 6 deg while the controller detailed above rendered a desired impedance. A trial was conducted for each combination of $K_d \in \{100, 200, 300, 400\}$ Nm/rad and $B_d \in \{0.0, 2.5, 5.0, 7.5\}$ Nms/rad, which were chosen to cover the ranges of stiffness and damping used in our walking controller [8]. The reaction torque supplied by the ankle joint was recorded. An example timeseries of the experiment is shown in Fig 4.

The timeseries data was regressed to a second order model with inertia $\hat{I}$, viscous damping $\hat{B}$ and stiffness $\hat{K}$ using least squares:

$$\hat{\tau}_\text{j} = \hat{K}\theta_\text{j} + \hat{B}\dot{\theta}_\text{j} + \hat{I}\ddot{\theta}_\text{j}. \tag{15}$$

The model torque $\hat{\tau}_\text{j}$, *i.e.* the torque that the modeled second-order system would produce subject to the same input, was calculated (magenta dashed line in Fig. 4). Fig. 5 shows the relationship between desired and observed stiffness and damping for each case. The VAF was calculated between the measured and modeled torque to assess the quality of the model (Fig 6). High VAF values indicate that the system dynamics were similar to a second order system.

Additionally, sinusoids were fit to the observed torque data at each amplitude and phase, allowing an empirical calculation of the system's frequency response for each condition. Fig 7 shows an example of this frequency response for the trial with $K_d = 200$ Nm/rad and $B_d = 7.5$ Nms/rad averaged over each displacement. By adding compensation, both the magnitude and phase response are closer to the desired behavior.

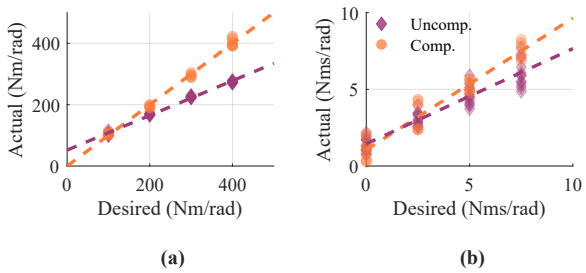

Fig. 5. Plots of the observed (a) joint stiffness $\hat{K}$ and (b) damping $\hat{B}$ as functions of desired values. By compensating for the drivetrain dynamics (orange circles), the joint impedance is closer to the desired values than the uncompensated (purple diamonds).

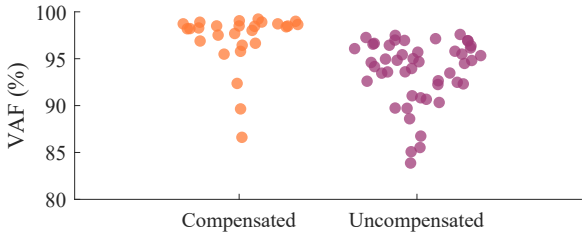

Fig. 6. A swarm chart of the variance accounted for (VAF) by a second order linear model for both the compensated and uncompensated system. Each point represents a trial of different desired stiffness, damping and displacement amplitude. The compensated system shows consistently higher VAF than the uncompensated system, showing that the compensation makes the system behave more like a second order system.

IV. Walking Trial Validation

To validate the controller's performance in more practical conditions, the ankle's joint impedance was identified during walking through a perturbation experiment, similar to [9], [10]. A hybrid kinematic impedance walking controller [8] was implemented on the OSL. This controller uses variable impedance control during stance and kinematic control during swing. The desired stance impedance trajectories given by the walking controller were converted into control gain trajectories using the impedance compensator presented in Section III, shown in Fig. 8. If our controller works, we should measure a stiffness around 340 Nm/rad at midstance.

A participant with an above-the-knee amputation (AKA) walked back and forth across a walkway with an embedded perturbation platform (MISTRAL, Symétrie, France). A forceplate (9260AA, Kistler, Switzerland) mounted to the top of the perturbation platform measured the ground reaction force, allowing for the calculation of the ankle torque. A 5 deg dorsiflexion ramp perturbation was applied randomly with 50% likelihood during midstance. VICON motion capture markers attached to the foot and shank of the prosthesis allowed for ankle joint angle calculations at 300 Hz.

The kinematic and kinetic data were segmented with 100 ms windows following each perturbation. The mean non-

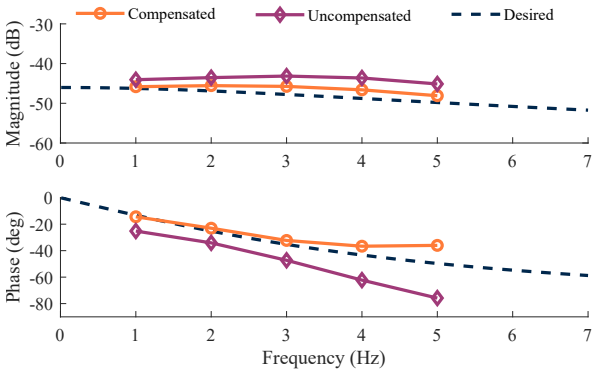

Fig. 7. An example frequency response plot of the observed and desired behavior for $K_d = 200$ Nm/rad, $B_d = 7.5$ Nms/rad averaged over the three tested amplitudes. By compensating for the drivetrain dynamics, both the magnitude and phase of the frequency response are improved.

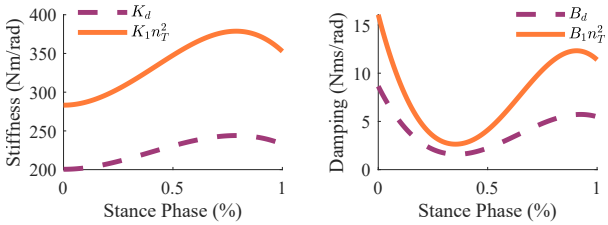

Fig. 8. Control trajectories of gains K_1 and B_1 (scaled up by n_T^2 for plotting) based on desired joint stiffness K_d and damping B_d for the ankle joint given by the walking controller [8].

perturbed data were subtracted from each perturbation trial to isolate the perturbation response. Each trial of timeseries data was regressed to a second order model, yielding ankle stiffness, damping, and inertia estimates (Fig. 9) (VAF = VALUE_TODO%).

V. Discussion and Conclusion

Acknowledgement

The authors thank Yunqing Yi and Guillermo Robles for their technical contributions to the perturbation system.

References

[1] A. F. Azocar, L. M. Mooney, J. F. Duval, A. M. Simon, L. J. Hargrove, and E. J. Rouse, "Design and clinical implementation of an open-source bionic leg," *Nat. Biomed. Eng.*, vol. 4, no. 10, pp. 941–953, 2020.

[2] M. R. Tucker, J. Olivier, A. Pagel, H. Bleuler, M. Bouri, O. Lambercy, J. R. Del Millán, R. Riener, H. Vallery, and R. Gassert, "Control strategies for active lower extremity prosthetics and orthotics: A review," *J. Neuroeng. Rehabil.*, vol. 12, no. 1, 2015.

[3] R. R. Torrealba and E. D. Fonseca-Rojas, "Toward the Development of Knee Prostheses: Review of Current Active Devices," *Appl. Mech. Rev.*, vol. 71, no. 3, pp. 1–22, 2019.

[4] F. Sup, H. A. Varol, and M. Goldfarb, "Upslope walking with a powered knee and ankle prosthesis: Initial results with an amputee subject," *IEEE Trans. Neural Syst. Rehabil. Eng.*, vol. 19, no. 1, pp. 71–78, 2011.

[5] A. F. Azocar and E. J. Rouse, "Characterization of Open-loop Impedance Control and Efficiency in Wearable Robots," *IEEE Robotics and Automation Letters*, vol. 7, pp. 4313–4320, 2022.

[6] C. Nesler, G. Thomas, N. Divekar, E. J. Rouse, and R. D. Gregg, "Enhancing Voluntary Motion With Modular, Backdrivable, Powered Hip and Knee Orthoses," *IEEE Robotics and Automation Letters*, vol. 7, no. 3, pp. 6155–6162, 2022.

[7] G. C. Thomas, J. S. Mehling, J. Holley, and L. Sentis, "Phase-Relaxed-Passive Full State Feedback Gain Limits for Series Elastic Actuators," *IEEE/ASME Transactions on Mechatronics*, vol. 26, no. 1, pp. 586–591, 2020.

[8] T. K. Best, C. G. Welker, E. J. Rouse, and R. D. Gregg, "Data-driven variable impedance control of a powered knee–ankle prosthesis for adaptive speed and incline walking," *IEEE Transactions on Robotics*, pp. 1–19, 2023.

[9] E. Rouse, L. Hargrove, E. Perreault, and T. Kuiken, "Estimation of human ankle impedance during the stance phase of walking," *IEEE Trans. Neural Syst. Rehabil. Eng.*, vol. 22, no. 4, pp. 870–878, 2014.

[10] A. L. Shorter and E. J. Rouse, "Mechanical impedance of the ankle during the terminal stance phase of walking," *IEEE Trans. Neural Syst. Rehabil. Eng.*, vol. 26, no. 1, pp. 135–143, jan 2018.

Figures/EstimatedWalkingKBI.pdf

Fig. 9. Estimated stiffness, damping, and inertia of the OSL ankle joint during midstance. Error bars indicate one standard deviation on either side of the mean.